RSC Advances

ROYAL SOCIETY OF CHEMISTRY

www.rsc.org/advances

Vertically and compactly rolled-up reduced graphene oxide film/epoxy composites: a two-stage reduction method for graphene-based thermal interfacial materials

Dong Han, Yun-Hong Zhao, Ya-Fei Zhang, Shu-Lin Bai*

Department of Materials Science and Engineering, HEDPS/CAPT/LTCS, Key Laboratory of Polymer Chemistry and Physics of Ministry of Education, College of Engineering, Peking University, Beijing 100871, China

Abstract Graphene-based thermal conductive composites have come into notice in recent years. A considerable number of works devoted to increase thermal conductivity by increasing the graphene loading. However, it is not practical for the fabrication process when the graphene content is too high. In this work, a novel fabrication method of graphene-based composite is proposed, by which thermal-reduced vertically aligned reduced graphene oxide (TR-VArGO)/epoxy composite was obtained. This method involves mainly two-step reduction of graphene oxide and hand-rolling process of reduced graphene oxide film. The thermal conductivity of TR-VArGO/epoxy composite is up to 2.645 W m^{-1} K^{-1}, i.e. an enhancement of as high as 887% compared to pure epoxy. By contrast, randomly distributed TR-rGO sheets/epoxy composite with the same rGO loading has a thermal conductivity of only 1.270 W m^{-1} K^{-1}. This difference is attributed to the vertical alignment of TR-VArGO films, which provides a rapid and effective heat-transfer path. This mechanism of high thermal conductivity is further confirmed

* Corresponding author. Tel.: +86-10-6275 9379.

E-mail address: slbai@pku.edu.cn (Shu-Lin Bai)

by theoretical prediction and finite element calculation. The results obtained indicate that the vertically aligned reduced graphene oxide/epoxy composite may become a good candidate of thermal interfacial materials.

1. Introduction

With the continuous development of modern microelectronic devices packed with highly integrated circuits, their increasing power densities have caused higher operating temperature, resulting in a significant bottleneck of heat dissipation in various micro-devices [1-6]. Great efforts have been made for the development of high-performance thermal interfacial materials (TIMs) based on carbon materials (e.g., diamond powders, graphite nanoplatelets, carbon nanotubes and carbon fibers) in order to break the bottleneck [4, 7-10]. Most of works devoted to improve thermal conductivity of polymeric composites by increasing carbon-fillers loading. However, the good dispersion of fillers and process ability of high filler mixture are always the target difficult to realize when the fillers content is too high.

Graphene, a surprising allotrope of carbon which is constitutive of only one plain layer of atoms arranged in a two-dimensional hexagonal lattice, exhibits an amount of intriguing unique properties, such as ultrafast electron mobility [11], super high mechanical strength [12], unusually good thermal conductivity [13-15] and ultralarge specific surface area [16]. Compared to carbon nanotubes, carbon blacks and other nanofillers, these unique properties make graphene become an incomparable material, which has been used in chemical sensors [17], microelectronic devices [18, 19], transparent & flexible electrically conductive films [20] and micro-supercapacitor for energy storage [21], etc. Besides, it is noteworthy that two dimensional graphite, graphene or graphene oxide (GO) are often used as fillers for polymeric composites to improve certain properties, such

as mechanical, electrical or thermal properties [4, 8, 22-26]. For instance, the thermal performance of graphite nanoplatelets/epoxy composites got better with increasing degree of graphite exfoliation [8]. In some cases, graphene are necessary to be assembled into specific architecture to implement certain features. A typical example is that graphene must be stacked in a 3-D porous structure in electrodes of electrical energy storage devices to promote rapid ion migration and make the utmost of its large specific surface area [16]. Hence, it's necessary to arrange graphene into particular structure so as to fulfill diverse functions. For TIMs, high thermal conductivity in the out-of-plane direction is expected [27, 28], so it's essential to assemble graphene into vertically aligned architecture to facilitate heat dissipation in the normal direction of contact solid interfaces. However, unlike carbon nanotube arrays [28], it's difficult or even impossible to grow vertically aligned graphene directly. On one hand, graphene is inclined to lean on substrates; on the other hand, direct growth method is in low yield and unavailable to large-scale applications. Therefore, a novel and simple approaches to vertically align graphene or reduced graphene oxide (rGO) are desired to increase out-of-plane thermal conductivity of TIMs.

Yoon et al. [29] reported a method to fabricate densely and vertically aligned reduced graphene oxide (VArGO). First, GO film was obtained by spontaneous evaporation overnight. Then the films were rolled manually to get vertically aligned architecture. Finally, VArGO film was formed by thermal annealing at the temperature up to 1000 °C for 1 h (0.14 °C/min). Herein, we report a more efficient and simple method to fabricate thermal-reduced VArGO (TR-VArGO)/epoxy composite, which has a high thermal conductivity of 2.645 W m^{-1} K^{-1}, i.e. an enhancement of as high as 887% compared to pure epoxy. This value is more than 2 times that of randomly distributed TR-rGO sheets/epoxy composite with the same rGO loading, indicating that the vertical alignment of continuous rGO film provides a rapid and effective heat-transfer

path to facilitate the heat dissipation. Furthermore, the heat-transfer mechanism of the composite is confirmed by theoretical prediction and finite element calculation.

2. Experimental

2.1 *Fabrication of rGO film and rGO sheets*

Well-dispersed GO aqueous solution (6 mg mL^{-1}) was prepared from graphite powder (Sinopharm Chemical Reagent Co., Ltd) with $NaNO_3$, H_2SO_4 and $KMnO_4$ using a modified Hummers method according to previous reports [21, 30].

rGO film was fabricated on zinc foil template at ambient temperature by interfacial-gel method [31]. The GO dispersion was diluted to 3 mg mL^{-1} with pre-made aqueous HCl solution (10^{-3} mol L^{-1}) and the mixture was ultrasonically agitated at the power of 100 W for 3 h. Zinc foil (Benchely) of 0.2 mm in thickness was immersed into acidified GO dispersion for interfacial gelation for 3 h. Then interfacial gel grown on zinc foil surface was completely washed with deionized water and then immersed in water for a period of 20-30 min so as to remove physically adsorbed GO platelets. Immediately following the washing step, the interfacial gel film was detached from zinc foil surface in 20 fold diluted HCl solution. The free-standing gel film was then transferred into aqueous HCl solution for another 5 h to dissolve residual Zn impurities. Finally, the prepared gel (rGO) film was immersed in deionized water for more than 12 h to remove acidic impurities. Furthermore, by sonicating at the power of 100 W for 5h in deionized water, some pieces of rGO films were exfoliated into rGO sheets which were collected for thermal reduction process after further vacuum freeze-drying.

2.2 *Fabrication of rGO/polyvinyl alcohol (PVA) composite film*

Before fabrication of rGO/PVA composite film, the rGO gel film was transferred from deionized water into 4 wt.% aqueous solution of PVA (PVA-124, Sinopharm Chemical Reagent

Co., Ltd, average molecular weight 105000 g mol^{-1}). Then the rGO film was kept in aqueous PVA solution at 50 °C for 1 h in order that the PVA molecules could fully diffuse into the porous architecture of rGO film. Next, the rGO film was moved on a piece of polyethylene glycol terephthalate (PET) membrane, hung up to remove redundant aqueous PVA solution, and dried at room temperature for 5 h. After thoroughly drying, it was easy to peel off the rGO/PVA composite film from the PET membrane, and the composite film was of sufficient strength to proceed the rolling-up process.

2.3 *Fabrication of vertically aligned rGO/PVA (VArGO/PVA) composite*

As-fabricated rGO/PVA composite film was cut into narrow strips (3 mm in width) prior to the rolling-up process. Then, the surface of these strips was slightly wetted with aqueous PVA solution (4 wt.%) to allow them to be tightly rolled. After vacuum freeze-drying, a strip was manually rolled up to get a VArGO/PVA composite disc sample with a diameter of 12.7 mm and thickness of 3 mm.

2.4 *Fabrication of thermal-reduced VArGO (TR-VArGO) and TR-rGO sheets*

TR-VArGO and TR-rGO sheets were formed by thermal reduction treatment which included a three-stage temperature-rise period and a 30 min-holding stage. The staged heating process was determined by the thermogravimetric (TG) curve of VArGO/PVA composite and was used to prevent excessive reduction of VArGO/PVA composite into rGO powder. As shown in Figure 1, the weight loss of VArGO/PVA composite was divided into three stages as follow: (I) from room temperature to 200 °C, the physically absorbed water of VArGO/PVA composite was evaporated [32]; (II) from 200 to 400 °C, PVA was decomposed into abundant CO and CO_2. Besides, CO and CO_2 were also released from the decomposion of anhydrides and phenols of

rGO [33]; (III) from 400 to 1000 °C, residual oxygen-containing functional groups in VArGO/PVA composite were removed steadily [34].

The thermal reduction process of the VArGO/PVA composite samples and rGO sheets is the same as follows: firstly, samples were put in a U-type quartz tube installed in a temperature programmable furnace (SGL-1200, Shanghai Daheng), then were heated from room temperature to 200 °C at the rate of 0.5 °C/min under an argon flow (100 s.c.c.m.); secondly, the temperature was increased from 200 to 400 °C at a slower ramp rate of 0.2 °C/min; thirdly, the samples were heated up to 1000 °C at the rate of 2 °C/min, and then the specific temperature was kept for 30 min under the same argon flow; finally, the furnace cooling was followed until room temperature to get pure TR-VArGO samples and TR-rGO sheets.

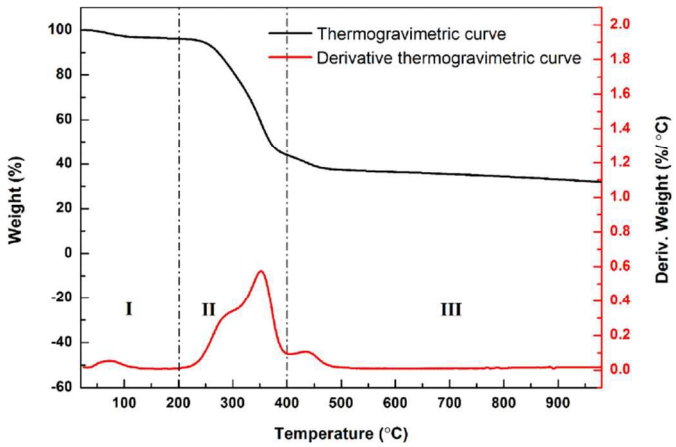

Figure 1. Thermogravimetric (TG) and derivative thermogravimetric (DTG) analysis of VArGO/PVA composite.

2.5 *Fabrication of TR-VArGO/epoxy and TR-rGO sheets/epoxy composites*

TR-VArGO/epoxy composite was prepared in suitable molds by infiltrating the as-fabricated TR-VArGO with liquid epoxy resin prepolymer and a viscous mixture of base and curing agent (diglycidyl ether of bisphenol A, E-51 and diethyltoluenediamine, 593#, Beijing great cause of

Pulin Chemical Co., Ltd, base/ curing agent = 4:1 in weight), followed by vacuum outgassing in a vacuum oven for 20 min and then thermally curing at 80 °C for 4 h to obtain the composite sample.

As for TR-rGO sheets/epoxy composite, first, 0.188 g TR-rGO sheets were dispersed in acetone and the mixture solution was agitated by ultrasonic treatment at the power of 100 W for 3 h. Then 0.8 g epoxy base agent was added into the mixture and mechanically stirred for 1 h, followed by adding 0.2 g curing agent and continually stirring for another 30 min at 50 °C to remove excess acetone. Final curing process of TR-rGO sheets/epoxy composite is identical to that of TR-VArGO/epoxy composite. In order to realize accurate measurements of thermal conductivity, the top and bottom surfaces of as-prepared TR-VArGO/epoxy and TR-rGO sheets/epoxy composites disc were slicked by slight and careful polishing and a final dimension of samples is 12.7 mm (diameter) × 2 mm (thickness).

2.6 *Characterization of materials*

The morphological and microstructural characterizations of as-obtained samples were performed using a field emission scanning electron microscope (FE-SEM, S-4800, HITACHI, Japan) operated at 10 kV. The detailed morphology of TR-rGO sheets was measured by transmission electron microscope (TEM, JEM-2100F, JEOL, Japan) at 200 kV. Chemical composition and structure characterizations of GO, metal-reduced rGO (MR-rGO), thermal-reduced rGO (TR-rGO) were performed. Energy dispersive spectroscopy (EDS) measurements were conducted on a Bruker X Flash Detector 5010 energy dispersive spectrometer. X-Ray powder diffraction (XRD) measurements were performed on a D8/Aduance X-ray diffractometer (BRUKER/AXS, Germany) with Cu Kα radiation in the range of 5-50°. Laser Raman spectroscopy was performed using HORIBA Jobin Yvon LabRAM HR Evolution Raman

spectrometer with He-Ne laser excited at 514.5nm with the power of 150 uw/cm^2. Fourier transform infrared spectroscopy (FT-IR) was measured on VECTOR 22 fourier transform infrared spectrometer (BRUKER/AXS, Germany). All X-ray photoelectron spectroscopy (XPS) measurements were conducted by Axis Ultra imaging photoelectron spectrometer (Kratos Analytical Ltd., Japan) with a monochromatic Al Kα X-ray source at 225 W.

2.7 *Thermal properties characterization*

Values of thermal conductivity were calculated from the equation $k = \alpha\rho C_p$, where k, α, ρ and C_p represent thermal conductivity, thermal diffusivity, material bulk density and specific heat capacity, respectively. Thermal diffusivity was measured by a laser flash apparatus (LFA 447 Nanoflash, NETSZCH, Germany). Bulk density was calculated from sample weight and volume. Specific heat capacity was obtained by a differential scanning calorimeter (DSC, Q2000, TA Instruments, America) with a heating rate of 10 °C/min from 0 to 100 °C. Dynamic thermogravimetric analysis was performed on a thermogravimetric Analyzer (Q600 SDT, TA Instruments, America) with a heating rate of 10 °C/min from room temperature to 900 °C in a nitrogen atmosphere.

3. Results and discussion

Generally, rGO film is formed by one-step thermal reduction of paper-like aligned GO film which is prepared by a vacuum assisted flow-filtration method [35, 36]. In order to increase the efficiency in the film-forming process, we transformed the reduction procedure into a two-stage process. This called two-stage reduction method is described in Figure 2. Firstly, according to a metal-templated interfacial-gel method reported by Maiti et al. [31], we prepared metal-reduced rGO (MR-rGO) film instead of GO film on zinc foil template. Meanwhile, to make sure that the as-prepared rGO film has sufficient strength to proceed the rolling-up process, it was immersed

into 4 wt.% aqueous solution of PVA, and after thoroughly dried, rGO/PVA composite film was formed. Due to the addition of PVA, this composite film with sufficient tensile strength can be cut into strips and rolled into VArGO/PVA composite with a packing density of 0.36 g/cm^3. In the following thermal reduction process, TR-VArGO was formed by a three-stage temperature-rise period and a 30 min-holding stage, yielding a packing density of 0.16 g/cm^3. Finally, TR-VArGO/epoxy composite was fabricated in suitable molds by infiltrating the as-made TR-VArGO with epoxy resin. The prepared TR-VArGO/epoxy composite can be used as TIMs to fill the voids and grooves created by imperfect surface finish of two mating surfaces, thus improving surface contact and ensuring a continuous path for the heat-transfer. Figure 2(F) shows two TIM layers used in integrated circuit, TIM-1 is inserted between the chip and the integrated heat spreader (IHS) while TIM-2 is used between IHS and the heat sink.

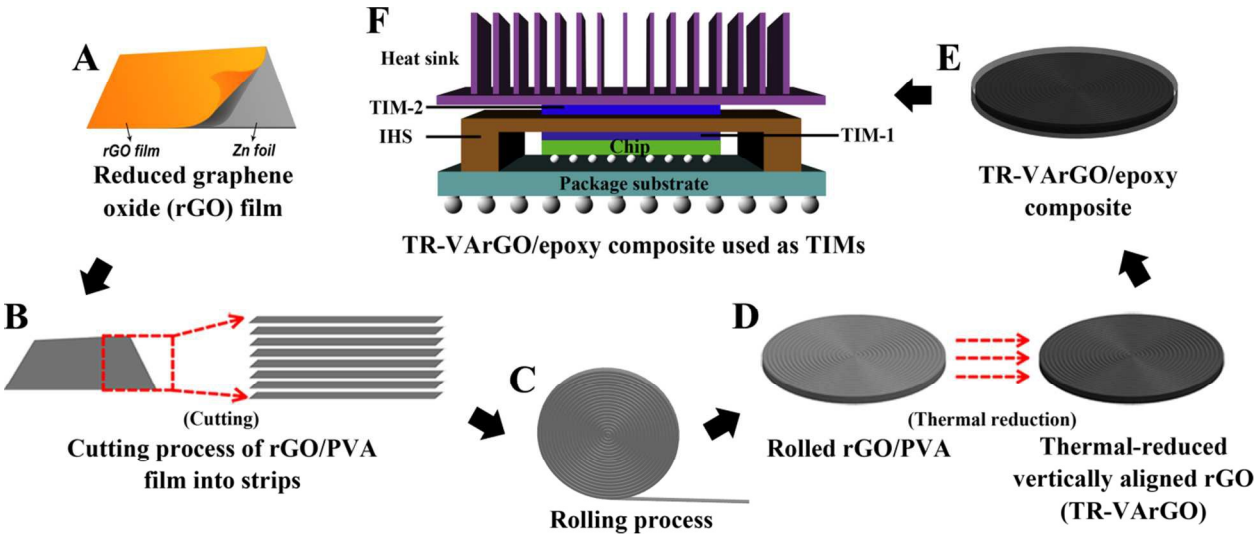

Figure 2. Schematic fabrication procedure of thermal-reduced vertically aligned reduced graphene oxide (TR-VArGO)/epoxy composite. (A) The free-standing rGO film was fabricated on zinc foil template at ambient temperature by interfacial-gel method [31]. (B) As-prepared rGO film was immersed into 4 wt.% aqueous solution of polyvinyl alcohol (PVA), and after thoroughly dried, it was cut into several narrow strips (3 mm in width). (C) Rolling process of

thin rGO/PVA composite strips. (D) The VArGO/PVA composite was reduced by a thermal reduction process to give TR-VArGO sample. (E) TR-VArGO/epoxy composite was fabricated in suitable molds by infiltrating the as-prepared TR-VArGO with epoxy resin. (F) TR-VArGO/epoxy composite was used as TIMs in integrated circuit (TIM-1 used between the chip and the integrated heat spreader (IHS), TIM-2 used between IHS and the heat sink).

3.1 *Morphologies and microstructures of TR-rGO sheets, VArGO/PVA composite and TR-VArGO*

The morphologies and microstructures of TR-rGO sheets, VArGO/PVA composite and TR-VArGO samples are shown in Figure 3. It is clearly seen in Figure 3a & b that the TR-rGO sheet is on the order of 8-10 μm in size and 1.4-3.4 nm in thickness (about 4-10 layers), and is transparent with some ripples and wrinkles, indicating that the TR-rGO sheet is quite thin and flexible. Figure 3c shows that the VArGO/PVA composite is densely piled after simple hand rolling process and vertically aligned films are stuck tightly together due to the addition of PVA. The arrows in Figure 3c point out some extended PVA filaments bridging a small amount of gaps between layers, resulting in a decreased packing density. Nevertheless, the gaps between layers can benefit the penetration of liquid polymer in the following fabrication of composite. Because PVA can be completely decomposed at about 600 °C [36], thus further thermal reduction of VArGO/PVA composite via a staged heating process up to 1000 °C removed all the PVA adhered on the surface of VArGO, and then pure TR-VArGO samples were obtained. From Figure 3d and inset, it can be seen that there is almost no differences between these two samples except for the decomposition of PVA, the vertically aligned architecture of VArGO was retained after high temperature thermal reduction. TR-VArGO is arranged densely and the thickness of single layer is about 10-15 μm.

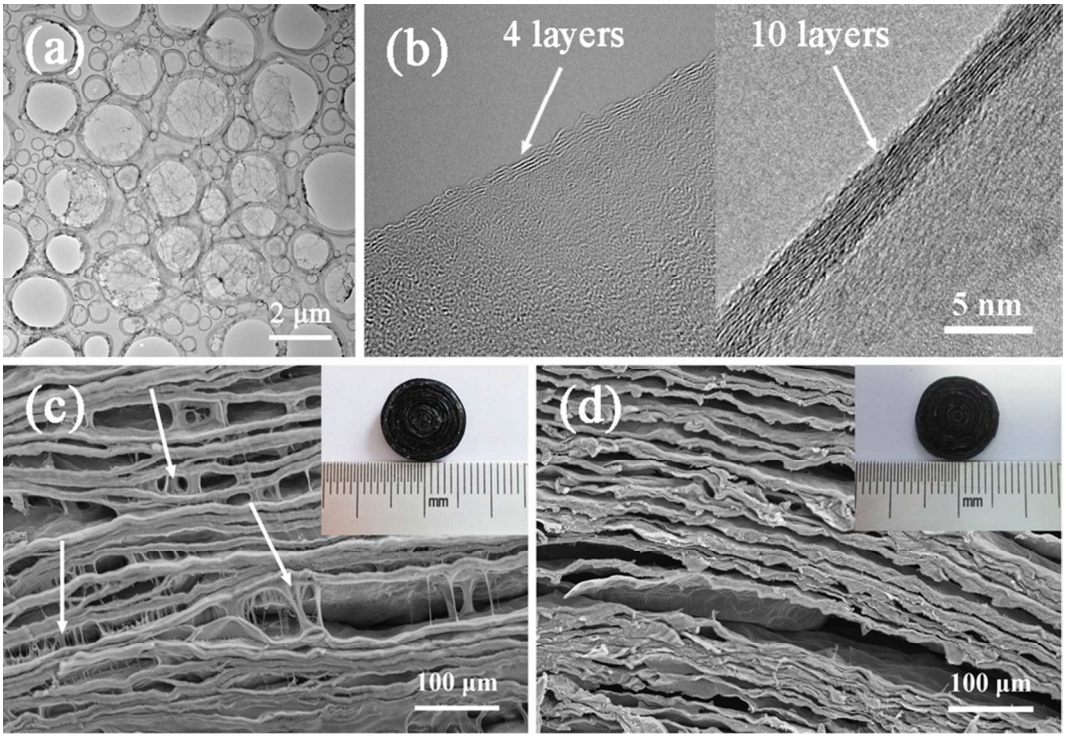

Figure 3. (a, b)TEM images of TR-rGO sheet. (c, d) SEM images of top surfaces of VArGO/PVA composite and TR-VArGO, respectivey. Insets showing the digital camera images of samples.

3.2 *Chemical composition and structure characterizations*

Two-stage reduction of GO removed most oxygen functional groups of itself to give highly reduced rGOs [31, 35-38], which is confirmed by the measurements of Fourier transform infrared spectroscopy (FT-IR), X-ray photoelectron spectroscopy (XPS), laser Raman spectroscopy and X-Ray powder diffraction (XRD). The oxygen content of GO illustrated in Table 1, which determined by low-resolution scanning XPS spectra, is as high as 54.70 at.% and that of rGO was reduced gradually with the progress of reduction. Furthermore, the element content is also confirmed by EDS (Table 2). As shown in FT-IR spectra (Figure 4a), the characteristic peaks appear for C=O (1730 cm^{-1}), aromatic C=C (1625 cm^{-1}), epoxy C–O–C (1224 cm^{-1}), and C–O (1054 cm^{-1}) in the GO spectrum [39], demonstrating that the graphite powder has high degree of

oxidation. After the zinc reduction, the peaks for oxygen functional groups are partially reduced, and the peak at 1224 cm^{-1} for epoxy C-O is nearly completely removed by the zinc reduction for 3 h. Further thermal treatment of MR-rGO at a temperature up to 1000 °C removed most of the residual oxygen-containing functionalities to give higher reductive degree thermal-reduced rGO (TR-rGO), it can be verified by the fact that the peaks at 1730 cm^{-1} for C=O and 1054 cm^{-1} for C-O became almost invisible compared to the MR-rGO spectrum. The remained strong δ C=C mode is ascribed to the effective repairing of conjugated C=C in sp^2 graphitic regions [40]. Furthermore, in the MR-rGO and TR-rGO spectrum, a distinct new peak at 1568 cm^{-1} appears and is attributed to the aromatic C=C group [41]. XPS was used to further quantitatively analyze the element content (Table 1) and chemical structure of GO, MR-rGO and TR-rGO. The deconvoluted XPS C1s spectra of these samples (Figure 4b) show three peaks for graphitic structure (C-C/C=C at 284.8 eV), hydroxyl/epoxy groups (C-O at 286.8 eV), and carbonyl group (O-C=O at 288.5 eV), respectively. The C-O bands come from epoxy and hydroxyl groups in the basal plane [35]. The C=O compounds mainly arose from single ketones [42] which decorates the edges of GO sheets but may also be bound to the basal plane as carbonyl groups [43, 44]. Compared to the XPS C1s spectrum of GO (Figure 4b), sharp decrease of the peak intensities for oxygen functional groups in the XPS C1s spectra of MR-rGO and TR-rGO indicates a high level reduction degree of GO after two-stage treatment. Moreover, the evolution of carbon bonds is also quantitated as shown in Table 3. It is obvious that the carbon sp^2 fraction increased with the progress of reduction, while the content of oxygen-containing functionalities (C-O and C=O) decreased.

Table 1 - Summary of the elemental compositions of materials.

Sample	C^a (%)	O^a (%)	d-spacing^b (Å)	$I_D/I_G{}^c$

GO	45.31	54.69	7.81	0.92
MR-rGO	82.04	17.96	3.75	1.89
TR-rGO	92.94	7.06	3.43	1.29

[a] Determined by low-resolution scanning XPS spectra. [b] Determined by XRD.

[c] Determined by Raman.

Table 2 - EDS results of the elemental composition of samples.

Sample	**Mass ratio (wt. %)**		**Atomic ratio (at. %)**	
	C	O	C	O
GO	49.37	50.63	56.50	43.50
MR-rGO	87.89	12.11	90.63	9.37
TR-rGO	95.24	4.76	96.38	3.62

Table 3 - Fitted binding energy (B.E.) and atomic ratio (at. %) of the C1s XPS spectra of samples

B.E. (eV)	**C1 (284.8)**	**C2 (286.8)**	**C3 (288.5)**
Assignment	C-C/C=C	C-O	O-C=O
GO	39.01	54.51	6.48
MR-rGO	64.49	28.48	7.03
TR-rGO	80.77	13.24	5.99

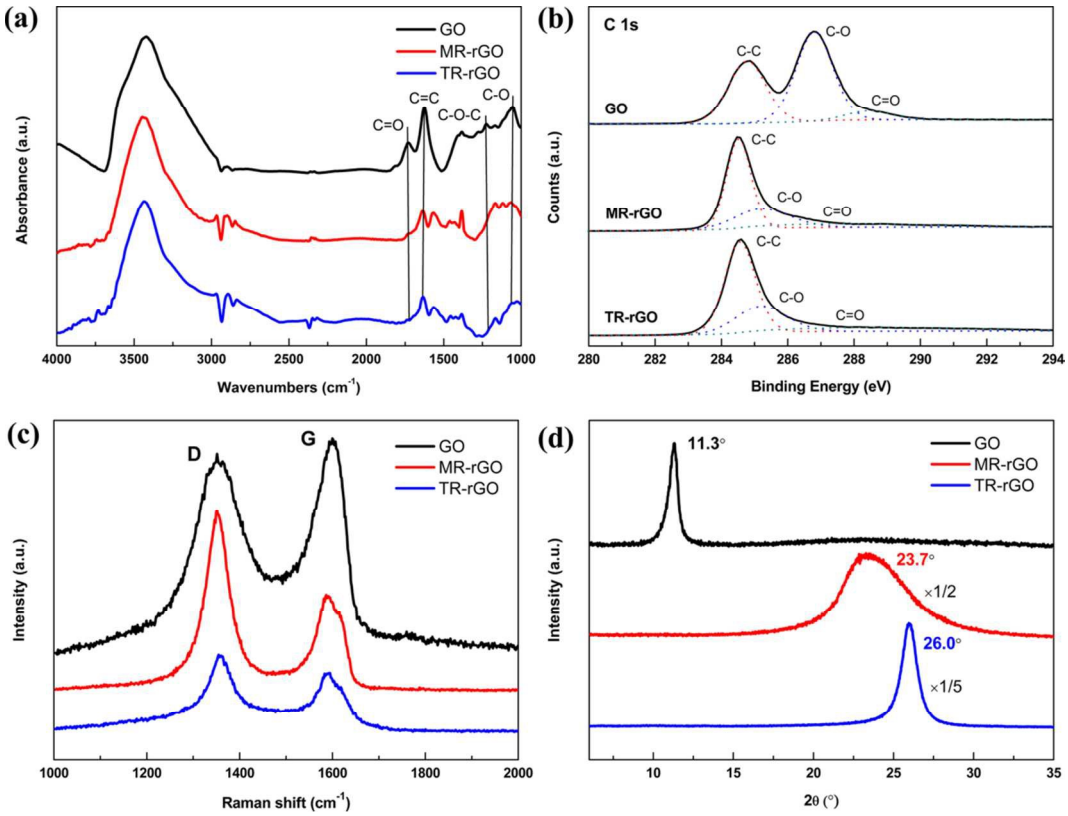

Figure 4. (a) FT-IR spectra, (b) XPS C1s spectra, (c) Raman spectra, (d) XRD patterns of GO, MR-rGO and TR-rGO.

Raman was performed to further investigate the texture of the samples. The Raman spectra of GO, MR-rGO and TR-rGO (Figure 4c) show two characteristic peaks at ~1352 cm^{-1} and ~1594 cm^{-1}, corresponding to D and G bands of graphene, respectively. As shown in Table 1, the ratio of ID/IG rises from 0.92 of GO to 1.89 of MR-rGO after the metal reduction, owing to an increase in structural defects which is attributable to the desorption of oxygen bonded saturated sp^3 carbons as CO_2 and/or CO (especially from epoxy groups) [45]. It is of vital importance to remove the oxygen contained in the GO during the reduction process, as sp^2 clusters in GO are isolated by oxygen atoms and a reduction by removal of O results in greater connectivity among the existing graphitic domains by the formation of new sp^2 domains [45, 46]. Surprisingly, a significant decrease in the ID/IG ratio from 1.89 to 1.29 is observed after thermal annealing

treatment, which is ascribed to the recovery of sp^2-hybridized carbon-carbon bonds of the graphitic lattice and connection of new sp^2 clusters in the samples through thermal treatment [47].

XRD was conducted to study the structure evolution of the samples. As shown in Figure 4d, a sharp peak appears at $2\theta = 11.3°$ corresponding to the (001) lattice plane in the pattern of GO, while it is nearly invisible in the patterns of MR-rGO and TR-rGO. However, there are two characteristic peaks at $2\theta = 23.7°$ and 26.0°, corresponding to the (002) plane in the other two rGO samples. According to the typical bulk graphite, presenting a diffraction peak at $2\theta = 27.0°$ [47], our final sample is in high graphitization degree. Additionally, from Table 1, it can be seen that the interlayer distance (*d*-spacing) of the samples decreased with the progress of reduction. The *d*-spacing ranges from 7.81 Å for GO to 3.43 Å for TR-rGO, which is attributed to the higher thermal exfoliation degree, higher reduction level, the decomposition of oxygen-containing functional groups and a better ordering of the two-dimensional sheets [35]. Compared to *d*-spacing of pristine bulk graphite (3.40 Å) [47], it is slightly larger for TR-rGO, this can be ascribed to the presence of a small amount of residual oxygen-containing functional groups or other structural defects [48]. From the above results, it's obviously that the TR-VArGO is homogeneously and densely piled by simple hand rolling, and it is in high reduction level after two-stage reduction treatment. As a result, we deduce that the as-prepared TR-VArGO/epoxy composite has high thermal conductivity in the normal direction.

3.3 *Morphology and microstructure of TR-VArGO/epoxy and TR-rGO sheets/epoxy composites*

Figure 5a&b shows the morphologies of top surface and longitudinal section of TR-VArGO/epoxy composite (the filler loading is 15.79 wt.%). It can be clearly seen in Figure 5a and inset that the arc-shaped rGO layers are embedded in epoxy matrix, i.e. the gaps between rGO layers (Figure 3b) are filled with epoxy, making TR-VArGO and epoxy be combined into a

uniform bulk material. Expectantly, there exist few of small crevices between rGO layers and epoxy matrix, indicating a good interface-bonding between filler and matrix. The cryo-fractured longitudinal section in Figure 5b also shows the layered and compact structure of this composite. Figure 5c displays the microstructure of cryo-fractured surface of TR-rGO sheets/epoxy composite with the same TR-rGO loading. It is noted that the TR-rGO sheets distribute randomly and densely in the epoxy matrix. Furthermore, the aggregation of TR-rGO sheets occurred and large-sized TR-rGO sheets were formed due to high filler content.

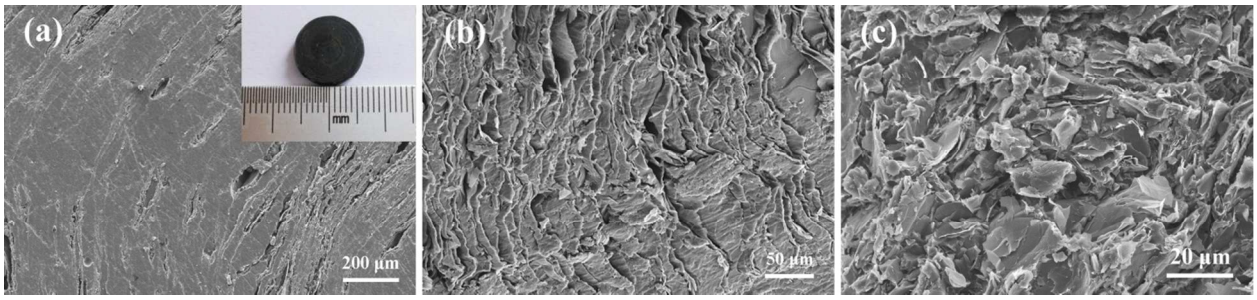

Figure 5. SEM images of (a, b) Top surface and longitudinal section of TR-VArGO/epoxy composite and (c) Cryo-fractured surface of TR-rGO sheets/epoxy composite. Inset showing the digital camera image of sample.

3.4 *Thermal Properties*

Thermal diffusivity of TR-VArGO/epoxy and TR-rGO sheets/epoxy composites was measured by a laser flash apparatus. To make a comparative analysis, thermal diffusivity of pure epoxy was also measured. Quantitative values of thermal diffusivity are given in Table 4. Furthermore, specific heat capacity was measured by a differential scanning calorimeter and bulk density was calculated from sample weight and volume.

Table 4 - Summary of detailed sample information and thermal properties

Sample	α	ρ	C_p	k	Mass

	(mm^2/s)	(g/cm^3)	(J g^{-1}K^{-1})	(W m^{-1}K^{-1})	fraction (wt.%)
Epoxy	0.164	1.152	1.456	0.275	-
TR-VArGO/epoxy	2.025	0.919	1.421	2.645	15.79
TR-rGO sheets/epoxy	1.004	0.897	1.410	1.270	15.80

As detailed in Table 4, the values of thermal conductivity and thermal diffusivity of as-prepared 15.79 wt.% TR-VArGO/epoxy composite are 2.645 W m^{-1} K^{-1} and 2.025 mm^2 s^{-1} (measured at 25 °C), i.e. 9.62 and 12.34 times that of pure epoxy, respectively. While, the corresponding values for random distributed TR-rGO sheets/epoxy composite are 1.270 W m^{-1} K^{-1} and 1.004 mm^2 s^{-1}, lower than the half values of TR-VArGO/epoxy composite, respectively. It is known that thermal conductivity is mainly determined by thermal diffusivity, which measures the ability of a material to conduct thermal energy relative to its ability to store thermal energy. To a large extent, the thermal conductivity enhancement of TR-VArGO/epoxy composite is primarily contributed by the vertical alignment of TR-rGO films.

In order to ascertain the thermal parameters of TR-VArGO, the parallel structure model determined by rule of mixture is proposed and combined with experimental results. Concerning the geometry shown in Figure 6, the effective thermal conductivity of composite is given by [49]:

$$k_{\text{par}} = k_1 f_1 + k_2 (1 - f_1) \quad (1)$$

where k_i and f_i are the thermal conductivity and volume fraction of the *ith* materials, respectively.

Due to the excellent surface polishing, it is quite apparent in the schematic diagram of Figure 6 that the parallel structure model can be perfectly applied to TR-VArGO/epoxy composite.

Hence, based on the experimental results of pure epoxy and TR-VArGO/epoxy composite (Table 4), it's fairly easy to obtain the thermal parameters of TR-VArGO using equation (1), which are detailed in Table 5.

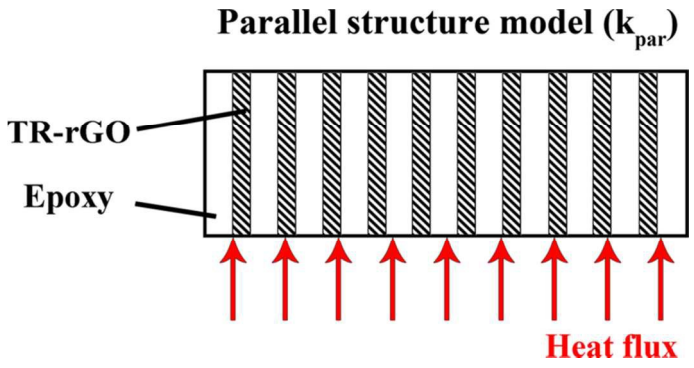

Figure 6. Thermal conductivity first-order models for TR-VArGO/polymer composite.

Table 5 - Summary of density and thermal properties of TR-VArGO

Sample	Density[a] (g/cm^3)	Specific heat capacity[a] ($J\ g^{-1}\ K^{-1}$)	Thermal diffusivity[b] (mm^2/s)	Thermal conductivity[c] ($W\ m^{-1}\ K^{-1}$)
TR-VArGO	0.442	1.147	14.786	7.496

[a] Calculated from experimental results.

[b] Calculated from experimental and theoretical results.

[c] Calculated by equation (1).

Based on the detailed thermal properties of TR-VArGO, the heat-transfer mechanism is quantitatively analyzed using finite element method. As shown in Figure 7a, a simple TR-VArGO/epoxy composite model is built. A strong anisotropy of TR-VArGO/polymer composite is evidenced by a distinguished architectural difference between in-plane and out-of-plane direction, here *r* defining in-plane direction, *Z* representing out-of-plane direction. According to

Liang et al. [50], aligned functionalized multilayer graphene sheets (fMGs) have high in-plane and low out-of-plane thermal conductivity. In real application of TIMs, out-of--plane thermal conductivity is often required and so measured in this work. In Figure 7b, TR-VArGO/epoxy composite is geometrically modeled to be composed of parallel TR-VArGO (red parts) embedded in epoxy matrix (blue parts). By using finite element method, the heat flux density profile across the composite sample is obtained in Figure 7b. Corresponding to the color bar, the heat flux density of TR-VArGO (red parts) is two orders of magnitude higher than that of epoxy (blue parts). So it's quite clear that almost all the heat flux travels preferentially through the TR-VArGO without thermal interface resistance between two different phases, which differs significantly from the heat-transfer mechanism of TR-rGO sheets/epoxy composite. Compared with vertical aligned TR-VArGO film, the random distribution of TR-rGO sheets in epoxy matrix causes two critical disadvantages. One is high thermal resistance at interface which is inclined at 0-90° angle to the heat flux direction. The other is the discontinuity of TR-rGO sheets which reduces the effectiveness of heat transfer in the material. Furthermore, Figure 7c exhibits a well-distributed temperature gradient profile, demonstrating a stable, reliable and high-efficiency heat-transfer process.

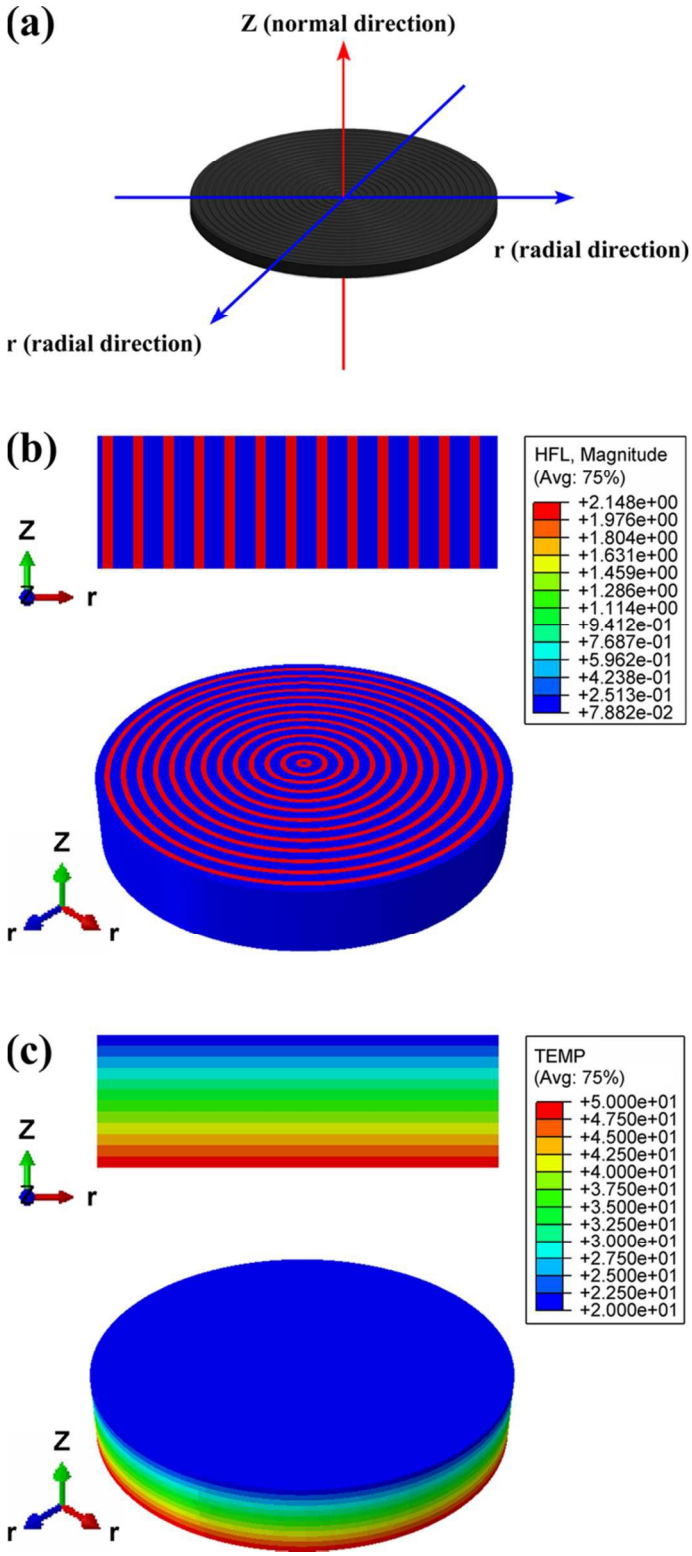

Figure 7. (a) An anisotropy schematic of TR-VArGO/epoxy composite. Normal direction *Z* and radial direction *r* are shown by the red and blue arrows, respectively. (b) Longitudinal section

and three-dimensional heat flux density and (c) temperature gradient profiles of TR-VArGO/epoxy composite.

Since the higher thermal conductivity of TR-VArGO/epoxy composite is primarily determined by the vertical alignment of TR-rGO films, the effect of TR-VArGO volume fraction on the thermal conductivity is further studied numerically and theoretically. As illustrated in Figure 8, the thermal conductivity increases linearly with increasing volume fraction of TR-VArGO. Meanwhile, two curves in Figure 8 are partially overlapping and show almost the same variation trend, demonstrating the accordance of parallel model and numerical simulation. Furthermore, the experimentally measured thermal conductivity values situate on or closely near the theoretical curve, but are slightly smaller than the numerical ones. For example, the measured conductivity is 2.645 W m^{-1} K^{-1} at the TR-VArGO volume fraction of 32.8 vol.%, i.e. 3% lower than the numerical value (2.725 W m^{-1} K^{-1}). The difference comes from the existence of small quantity of pores in real composite, while numerical calculation assumes the perfect microstructure of composite. It is confirmed by the longitudinal section view of Figure 5b that there are some irregular pores existing in the composite, increasing thermal resistance and hindering heat conduction in the normal direction.

From the theoretical and numerical results, it can be concluded that TR-VArGO/epoxy composite has a simple heat-transfer mechanism dominated by the elements with high thermal conductivity (TR-VArGO). Furthermore, a revelation is that the elements with high thermal conductivity must be stacked compactly and parallel to the heat flow direction to get high thermal conductivity.

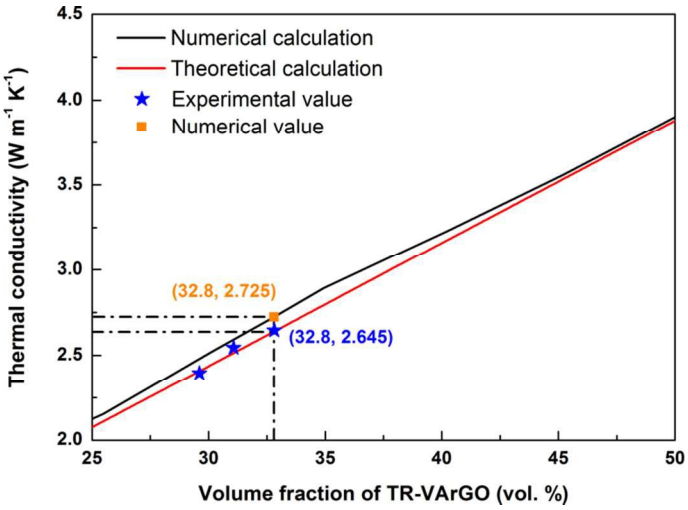

Figure 8. Thermal conductivities of TR-VArGO/epoxy composite as a function of volume fraction of TR-VArGO.

3.5 *Comparison with Reported Results*

Graphene is an optimal thermal conductive filler in polymeric composite due to its ultrahigh thermal conductivity (~5300 W m^{-1} K^{-1} for a suspended single-layer graphene) [14] and ease of assembly. However, efficient heat dissipation process requires a heat transfer pathway established by a large number of interconnected graphene nanoplatelets. Graphene nanoplatelets loading must reach a certain level in order to construct a three-dimensional interconnected heat-transfer network. Great efforts have been made on preparation of graphene filled polymer composites by increasing the loading of graphene. However, the favorable dispersion of filler cannot be guaranteed when the filler loading is too high, which causes a sensible reduction in thermal conductivity. Moreover, the poor processability of high filler composite materials is unlikely to meet the requirements in real industrial production processes. This work gives a novel approach for the high-efficiency fabrication of TR-VArGO, as well as TR-VArGO/epoxy composite. High thermal conductivity (2.645 W m^{-1} K^{-1}) and thermal conductivity enhancement

(887%) of TR-VArGO/epoxy composite are obtained at a moderate graphene weight fraction (15.79 wt.%).

For the purpose of comparison, our results and those of state-of-the-art graphene filled polymer composites are illustrated together in Figure 9. It is noticed that most of graphene-based polymer composites reported in literatures show the increasing thermal conductivity with increasing graphene loading as much as possible. Sun et al. [52] obtained an effective thermal conductivity of ~1.98 W m^{-1} K^{-1} at the optimum lateral dimensions (~200-400 μm) of graphite nanoplatelets (loading 10 wt.%). Song et al. [53] fabricated graphene-based epoxy composites at low cost and with environmentally friendly processing techniques and obtained a high thermal conductivity of 1.53 W m^{-1} K^{-1}, as well as a large thermal conductivity enhancement of 670% at a low filler loading (10 wt.%). Yu et al. [8] improved the thermal conductivity of graphite nanoplatelet/epoxy composite to 6.44 W m^{-1} K^{-1} by increasing the filler loading to 40 wt.%. Unlike other reporters, Ji et al. [51] applied ultrathin-graphite foams with weight fraction as low as 4.8 wt.% in a phase change material (wax) instead of dispersing large-amount high thermal conductivity graphene flakes or nanotubes to increase thermal conductivity of composites and reported a thermal conductivity of ultrathin-graphite foams/wax composite measured by self-electrical-heating steady state technique is ~1.65 W m^{-1} K^{-1}. As illustrated in Figure 9, TR-VArGO/epoxy composite has high thermal conductivity and thermal conductivity enhancement, elucidating that it's especially necessary to arrange graphene or reduced graphene oxide into particular architecture so as to take advantage of its high in-plane thermal conductivity. However, there still existing other graphene-based composites has higher thermal conductivity than TR-VArGO/epoxy composite, it may result from their high thermal conductivity and weight fraction

of additive graphene. Hence, we get a revelation that it's especially necessary to increase the fillers' thermal conductivity and weight fraction in our future work.

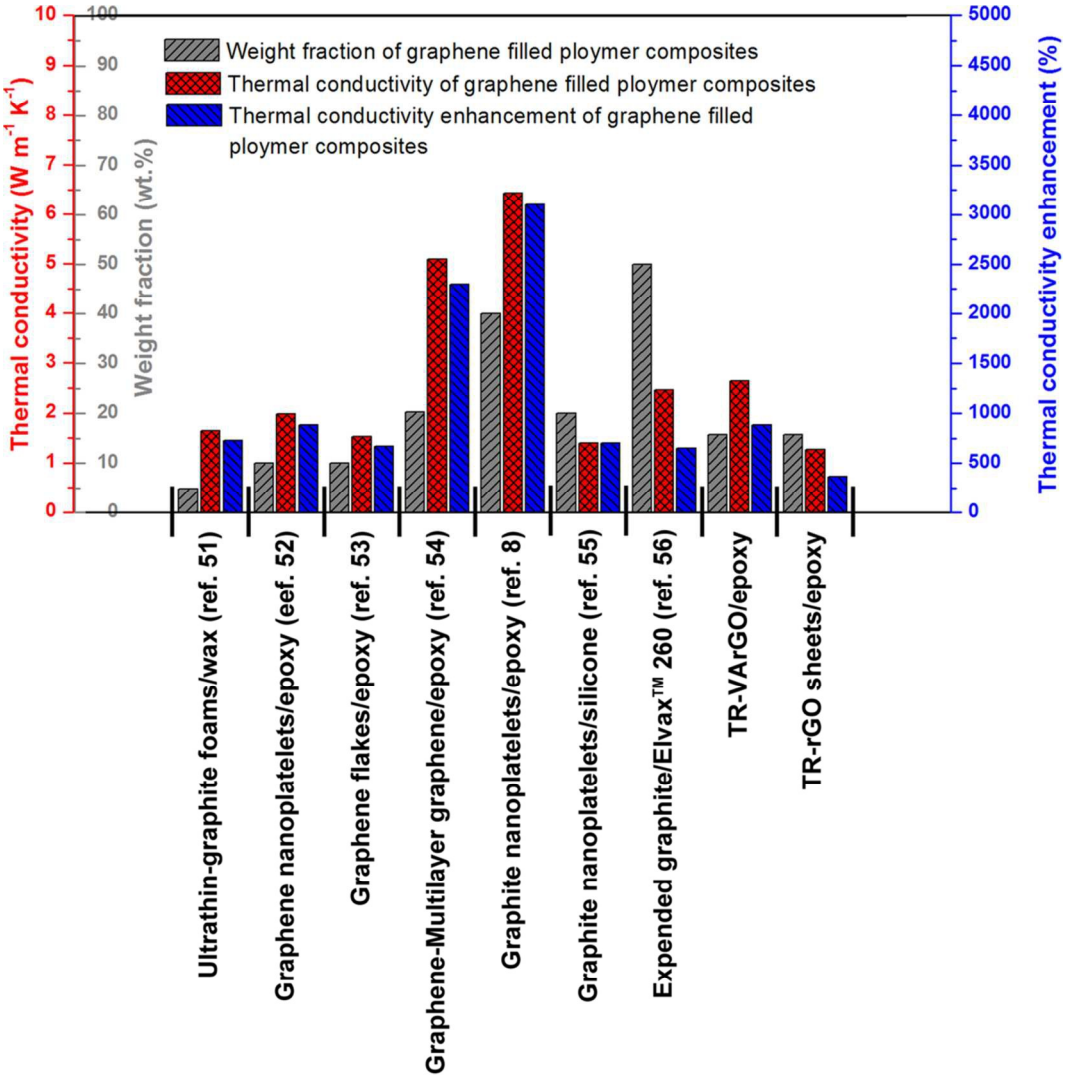

Figure 9. Comparison of weight fraction, thermal conductivity and its enhancement of graphene filled polymer composites between results in literature and in this work.

4. Conclusions

In summary, a two-stage reduction method and a simple rolling process were proposed to prepare vertically and compactly aligned reduced graphene oxide (VArGO)/epoxy composite. A high reduction level of thermal-reduced VArGO (TR-VArGO) is achieved using the two-stage

method. The rolling process guarantees the vertical and compact alignment of TR-VArGO film in the composite. The thermal conductivity of TR-VArGO/epoxy composite is up to 2.645 W m^{-1} K^{-1} and the thermal conductivity enhancement is as high as 887%. While, randomly distributed TR-rGO sheets/epoxy composite with the same TR-rGO loading has a thermal conductivity of 1.270 W m^{-1} K^{-1}, lower than the half value of TR-VArGO/epoxy composite. This difference is attributed to the vertical alignment of TR-VArGO films. By theoretical modelling and finite element simulation, it is revealed that the alignment of continuous graphene film provides a rapid and effective heat-transfer path to facilitate the heat dissipation. The high performance of TR-VArGO/epoxy composite synthesized by a simple and facile process in this work shows promising potentials in thermal management of microelectronic devices and photonic applications.

Acknowledgment

The authors would like to thank the support by NSFC and NSFC-RGC Joint Research Scheme (Nos. 11272008, 11361161001, 11202005 and CUHK450/13).

Notes and references

1 R. Prasher, *Proc. IEEE*, 2006, **94**, 1571.

2 A. A. Balandin, *Nat. Mater.*, 2011, **10**, 569.

3 A. J. McNamara, Y. Joshi and Z. M. Zhang, *Int. J. Therm. Sci.*, 2012, **62**, 2.

4 A. Yu, P. Ramesh, X. B. Sun, E. Bekyarova, M. E. Itkis and R. C. Haddon, *Adv. Mater.*, 2008, **20**, 4740.

5 S. Ganguli, A. K. Roy and D. P. Anderson, *Carbon*, 2008, **46**, 806.

6 K. M. F. Shahil and A. A. Balandin, *Solid State Commun.*, 2012, **152**, 1331.

7 Y. Zhang, X. Hu, J. H. Zhao, K. Sheng, W. R. Cannon, X. Wang and L. Fursin, *IEEE T. Compon. Pack. T.*, 2009, **32**, 716.

8 A. Yu, P. Ramesh, M. E. Itkis, E. Bekyarova and R. C. Haddon, *J. Phys. Chem. C*, 2007, **111**, 7565.

9 J. Hong, J. Lee, C. K. Hong and S. E. Shim, *Curr. Appl. Phys.*, 2010, **10**, 359.

10 Y. M. Chen and J. M. Ting, *Carbon*, 2002, **40**, 359.

11 K. I. Bolotin, K. J. Sikes, Z. Jiang, M. Klima, G. Fudenberg , J. Hone, P. Kima and H. L. Stormer, *Solid State Commun.*, 2008, **146**, 351.

12 C. Lee, X. Wei, J. W. Kysar and J. Hone, *Science*, 2008, **321**, 385.

13 S. Berber, Y. K. Kwon and D. Tománek, *Phys. Rev. Lett.*, 2000, **84**, 4613.

14 A. A. Balandin, S. Ghosh, W. Bao, I. Calizo, D. Teweldebrhan, F. Miao and C. N. Lau, *Nano Lett.*, 2008, **8**, 902.

15 I. Calizo, A. A. Balandin, W. Bao, F. Miao and C. N. Lau, *Nano Lett.*, 2007, **7**, 2645.

16 M. D. Stoller, S. Park, Y. Zhu, J. An and R. S. Ruoff, *Nano Lett.*, 2008, **8**, 2498.

17 C. Berger, Z. Song, T. Li, X. Li, A. Y. Ogbazghi, R. Feng, Z. Dai, A. N. Marchenkov, E. H. Conrad, P. N. First and W. A. de Heer, *J. Phy.. Chem B*, 2004, **108**, 19912.

18 M. C. Lemme, T. J. Echtermeyer, M. Baus and H. Kurz, *IEEE Electron Dev. Lett.*, 2007, **28**, 282.

19 Y. M. Lin, A. Valdes-Garcia, S. J. Han, D. B. Farmer, I. Meric, Y. Sun, Y. Wu, C. Dimitrakopoulos, A. Grill, P. Avouris and K. A. Jenkins, *Science*, 2011, **332**, 1294.

20 G. Eda, G. Fanchini and M. Ghhowalla, *Nat. Nanotechnol.*, 2008, **3**, 270.

21 Z. K. Wu, Z. Lin, L. Li, B. Song, K. Moon, S. L. Bai and C. P. Wong, *Nano Energy*, 2014, **10**, 222.

22 M. Fang, K. Wang, H. Lu, Y. Yang and S. Nutt, *J. Mater. Chem.*, 2009, **19**, 7098.

23 H. Bai, Y. Xu, L. Zhao, C. Li and G. Shi, *Chem. Commun.*, 2009, **13**, 1667.

24 Z. Chen, C. Xu, C. Ma, W. Ren and H. M. Cheng, *Adv. Mater.*, 2013, **25**, 1296.

25 S. Y. Kim, Y. J. Noh and J. Yu, *Compos. Part A-Appl. S.*, 2015, **69**, 219.

26 Z. H. Zhao, Z. K. Wu and S. L. Bai, *Compos Part A-Appl. S.*, 2015, **72**, 200.

27 Q. Ngo, B. A. Cruden, A. M. Cassell, G. Sims, M. Meyyappan, J. Li and C. Y. Yang, *Nano Lett.*, 2004, **4**, 2403.

28 J. Xu and T. S. Fisher, *Int. J. Heat Mass Transfer*, 2006, **49**, 1658.

29 Y. Yoon, K. Lee, S. Kwon, S. Seo, H. Yoo, S. Kim, Y. Shin, Y. Park, D. Kim, J. Y. Choi and H. Lee, *ACS Nano*, 2014, **8**, 4580.

30 Jr W. S. Hummers and R. E. Offeman, *J. Am. Chem. Soc.*, 1958, **80**, 1339.

31 U. N. Maiti, J. Lim, K. E. Lee, W. J. Lee and S. O. Kim, *Adv. Mater.*, 2013, **26**, 615.

32 M. A. Raza, A. Westwood, A. Brown, N. Hondow and C. Stirling, *Carbon*, 2011, **49**, 4269.

33 J. A. Menéndez, J. Phillips, B. Xia and L. R. Radovic, *Langmuir*, 1996, **12**, 4404.

34 K. P. Loh, Q. Bao, P. K. Ang and J. Yang, *J. Mater. Chem.*, 2010, **20**, 2277.

35 N. J. Song, C. M. Chen, C. Lu, Z. Liu, Q. Q. Kong and R. Cai, *J. Mater. Chem. A*, 2014, **2**, 16563.

36 Q. Q. Kong, Z. Liu, J. G. Gao, C. M. Chen, Q. Zhang, G. Zhou, Z. C. Tao, X. H. Zhang, M. Z. Wang, F. Li and R. Cai, *Adv. Funct. Mater.*, 2014, **24**, 4222.

37 B. Zhao, P. Liu, Y. Jiang, D. Pan, H. Tao, J. Song, T. Fang and W. Xu, *J. Power Sources*, 2012, **198**, 423.

38 Y. Yoon, S. Seo, G. Kim and H. Lee, *Chem. Eur. J.*, 2012, **18**, 13466.

39 D. Li, M. B. Müller, S. Gilje, R. B. Kaner and G. G. Wallace, *Nat. Nanotechnol.*, 2008, **3**, 101.

40 C. M. Chen, Q. Zhang, M. G. Yang, C. H. Huang, Y. G. Yang and M. Z. Wang, *Carbon*, 2012, **50**, 3572.

41 W. Chen and L. Yan, *Nanoscale*, 2010, **2**, 559.

42 G. Xie, Z Wang, Z. Cui and Y. Shi, *Carbon*, 2005, **43**, 3181.

43 W. Cai, R. D. Piner, F. J. Stadermann, S. Park, M. A. Shaibat, Y. Ishii, D.Yang, A. Velamakanni, S. J. An, M. Stoller, J. An, D. Chen and R. S. Ruoff, *Science*, 2008, **321**, 1815.

44 T. Szabó, O. Berkesi, P. Forgó, K Josepovits, Y. Sanakis, D. Petridis and I. Dékány, *Chem. Mater.*, 2006, **18**, 2740.

45 C. Mattevi, G. Eda, S. Agnoli, S. Miller, K. A. Mkhoyan, O. Celik, D. Mastrogiovanni, G. Granozzi, E. Garfunkel and M. Chhwalla, *Adv. Funct. Mater.*, 2009, **19**, 2577.

46 H. Wang, J. T. Robinson, X. Li and H. Dai, *J. Am. Chem. Soc.*, 2009, **131**, 9910.

47 C. Vallés, J. D. Núñez, A. M. Benito and W. K. Maser, *Carbon*, 2012, **50**, 835.

48 H. Chen, M. B Müller, K. J. Gilmore, G. G. Wallace and D. Li, *Adv. Mater.*, 2008, **20**, 3557.

49 M. Idicula, A. Boudenne, L. Umadevi, L. Ibos, Y. Candau and S. Thomas, *Compos. Sci. Technol.*, 2006, **66**, 2719.

50 Q. Liang, X. Yao, W. Wang, Y. Liu and C. P. Wong, *ACS Nano*, 2011, **5**, 2392.

51 H. Ji, D. P. Sellan, M. T. Pettes, X. Kong, J. Ji, L. Shi and R. S. Ruoff, *Energ. Environ. Sci.*, 2014, **7**, 1185.

52 X. Sun, P. Ramesh, M. E. Itkis, E. Bekyarova and R. C. Haddon, *J. Phys. Condens. Matter*., 2010, **22**, 334216.

53 S. H. Song, K. H. Park, B. H. Kim, Y. M. Choi, G. H. Jun, D. J. Lee, B. S. Kong, K. W. Paik and S. Jeon, *Adv. Mater.*, 2013, **25**, 732.

54 K. M. F. Shahil and A. A. Balandin, *Nano Lett.*, 2012, **12**, 861.

55 M. A. Raza, A. V. K. Westwood and C. Stirling, *Int. Symp. Adv. Packag. Mater. Microtech.*, 2010, 34.

56 S. Ghose, K. A. Watson, D. C. Working, J. W. Connell, Jr J. G. Smith and Y. P. Sun, *Compos. Sci. Technol.*, 2008, **68**, 1843.

Table of contents

Schematic fabrication procedure of thermal-reduced vertically aligned reduced graphene oxide (TR-VArGO)/epoxy composite.

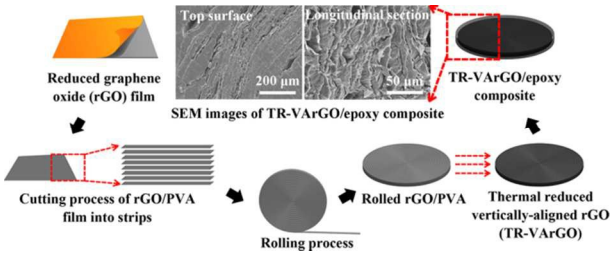

An efficient and simple method includes two reduction stages to fabricate thermal-reduced VArGO (TR-VArGO)/epoxy composite.